VISUALIZATION OF TWO- AND THREE-PHASE FLOW IN FRACTURES USING X-RAY COMPUTED TOMOGRAPHY

Freddy E. Alvarado[1], Abraham S. Grader[2] , Phillip M. Halleck[2]
[1]British Petroleum, Av. Francisco de Miranda. Edif. Centro Seguros Sudamerica, Piso 5. Caracas, Venezuela.
[2]The Pennsylvania State University, 203 Hosler, University Park, PA 16802, USA.

This paper was prepared for presentation at the International Symposium of the Society of Core Analysts held in Trondheim, Norway 12-16 September, 2006

ABSTRACT

Characterizing fracture morphology is necessary for accurate simulation of multiphase transport in fractured rocks. Although ambient-stress methods for obtaining fracture morphology exist, methods used in previous research lack the ability to map fracture closure as a function of stress or the distribution of immiscible phases within the fracture. Twenty-five-millimeter cylindrical sandstone samples were artificially fractured in tension and placed under confining stress in an x-ray-transparent vessel. The fracture morphology was characterized under dry conditions using high-resolution x-ray computed tomography at three successively higher applied closure stresses. Three immiscible fluids, water, benzyl alcohol and decane were injected into the fracture to emulate the phases present in an oil reservoir. The fluid-filled fracture was scanned under two- and three-phase conditions after various forced drainage processes were imposed. Such processes represent enhanced recovery techniques used in mature oil fields and are critical in understanding the role of fractures in secondary and tertiary recovery projects.

The results shown in this paper illustrate the ability of high-resolution x-ray CT to resolve changes in asperity contact area, fracture volume and fracture rugosity, and fracture morphology as a function of closure stress. These data can be correlated with measured flow impedance and used as input data for model development. In addition, the data are partitioned to extract the fracture volume and the portions of it occupied by separate fluid phases. The results presented here reveal how distribution of immobile phases acts to block flow of additional phases. Again, maps of fluid occupancy can be correlated with effective fracture permeability to aid in multi-phase model development.

INTRODUCTION

Multiphase flow in fractures is an important phenomenon that has been studied in several fields, including the oil industry, nuclear engineering, ground water hydrology, and the geothermal industry. There is still a lack of fundamental understanding of the mechanical and hydraulic response of fractures including fluid interactions with each other, the fracture walls, and the porous matrix. In early investigations, single phase flow through

fractures was simulated using two parallel glass plates. Lomize (1951) and Louis (1969) are recognized as the fathers of the well known cubic law, which relates flow rate, hydraulic head and fracture aperture. However, it does not take into account the rugosity of the fractures. Despite data under specific circumstances that support the cubic law, Witherspoon (1976), in general the complex geometry of real fractures makes it untenable. The principle experimental limitation has been the inability to characterize the fracture geometry with sufficient accuracy while performing flow tests under applied closure stress. Characterization of fracture aperture has been performed using both destructive and nondestructive methods. The destructive methods include injection of epoxy or metal, e.g. Tsang *et al*. (1987), surface topography measurements, Gentier *et al*. *(*1986), and casting of the fracture faces, Yeo *et al*. (1998). These methods all suffer from the inability to characterize the fracture under more than one stress condition and, worse, the inability to collect associated flow data under more than a single condition.

The nondestructive methods are magnetic resonance and x-ray CT. Durham (2001) carried out experimental work to examine the relationship between local rate of dissolution and local aperture during flow of a slightly acid aqueous solution through a fracture. They recognized the potential of CT scans to monitor changes in fracture morphology, but pointed to a lack of spatial resolution (1-mm maximum voxel resolution) with the medical CT scanners available at the time. However, industrial high-resolution x-ray CT can easily produce voxel sizes of 25 microns on 1-inch diameter samples, making possible *in situ* characterization of modest-aperture fractures.

A second factor holding back understanding of fracture flow is that most studies have been performed under single-phase conditions, not considering interactions between immiscible phases or capillary effects. High-resolution x-ray CT can also be used to map the occupancy of individual fluid phases within the fracture by calibrating image analysis techniques to the registration characteristics of each fluid phase present. Alvarado (2004) performed two-phase flow experiments in tensile fractures, highlighting the importance of fracture topology and phase occupancy on fracture conductivity. In this paper we describe the application and analysis of high-resolution x-ray CT to map both the geometry of a fracture and the distribution of two and three immiscible phases within the fracture under variable flow and closure stress conditions.

EXPERIMENTAL METHODS AND PROCEDURES

Fracture Preparation

The rock samples used were Berea Sandstone cores with average permeability (prior to fracturing) of about 100 mD. Separate samples were oriented with the bedding planes both perpendicular and parallel to the tensile fracture. Starting at 5-cm diameter, the cores were ground to precision cylinders. A modified (lengthened) Brazilian test fixture was used to create cross-diameter tensile fractures along the cores. Each sample was then over-cored to a 2.5 cm diameter, preserving the fracture along the length of the core. This over-coring process was used to eliminate any multiple fractures at the sample perimeter that might create bypassing flow channels. Finally the ends of the fractured

core were surface ground to avoid uneven stress loading at the flow distributors. The final dimensions of the cores were approximately 2.5 cm diameter and 7.5 cm length.

The three fluids used were water tagged with NaI (20%), decane tagged with iodo-dodecane (25%) and benzyl alcohol, Alvarado *et al. (*2004). These fluids present a clear contrast in x-rays attenuation, allowing the partitioning of the phases in the fracture. The immiscibility of the three fluids resembles the interaction of the fluids present in a reservoir, with benzyl alcohol representing an intermediate-wetting oil phase and decane a non-wetting gas phase.

Core Holders and Flow Distributors

A polycarbonate plastic core holder was used for experiments at low confining pressure (200 kPa) and a carbon-composite/aluminum vessel for high-pressure experiments (17 MPa). End-plug flow distributors were designed to allow the simultaneous injection of two phases into a tensile fracture. These end-plugs have separate ports for measuring fluid pressure at each end of the sample. The separate fluid phases are delivered directly to the face of the flow distributor from a two-cylinder computer-controlled precision syringe pump system.

X-ray CT Facility

The high-resolution x-ray CT facility is a third-generation scanner in which the source and detector are fixed and the scanned object rotates. The system has a 225-kV micro-focus x-ray generator and a 225-mm diameter image intensifier. Magnification can be adjusted by moving the object towards or away from the x-ray source. The highest theoretical resolution that can be obtained by the micro-focus source is 5 microns, limited by the focal-spot diameter.

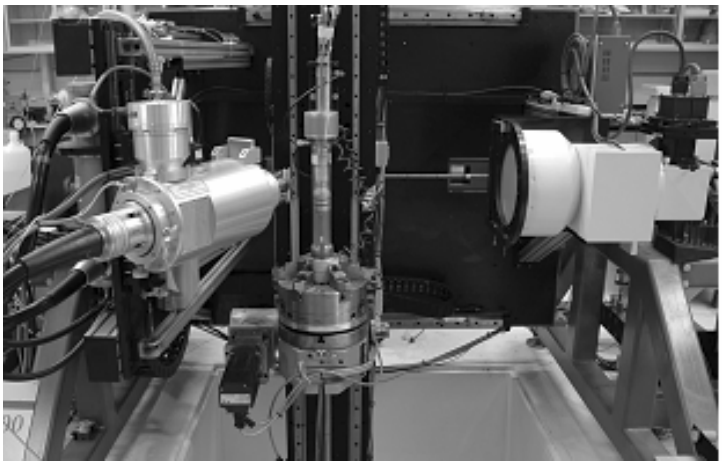

Figure 1: The core holder containing the Berea sample in the X-ray CT facility during three-phase flow experiments.

Figure 1 shows the CT facility during a multiphase flow experiment. The core assembly is vertical with upward flow. The injection and recovery plumbing (not shown in the photograph) allow the sample to rotate a full 360 degrees during scanning. X-rays pass through the vessel and sample to reach the image intensifier, which converts x-ray energy into a form of light that the digital camera can record. The digitized data are sent to a computer and converted into “raw” files (sinograms) that are then processed into images. Since the detector array is 1024 pixels across, the practical voxel dimensions are

approximately 1/1000 of the object diameter. The diameter of the core was 25 mm, leading to pixel resolution of 25 microns. Sequential images form a three-dimension virtual core, including the fracture structure.

RESULTS AND ANALYSIS

Fracture Aperture

The entire dry sample was scanned at a resolution of about 25 microns, resulting in a virtual three-dimensional core. The fracture was distinguished by its low CT registration shown as the dark linear feature in Figure 2 (center). The extracted center portion of the image, shown at the right of Figure 2, reduces the computational load without losing any part of the fracture. The initial slices consisted of 1024 x 1024 matrices. The extracted ones were reduced to 860 x 140, a size reduction of about an order of magnitude. A threshold process was then used to extract all connected voxels that form the fracture.

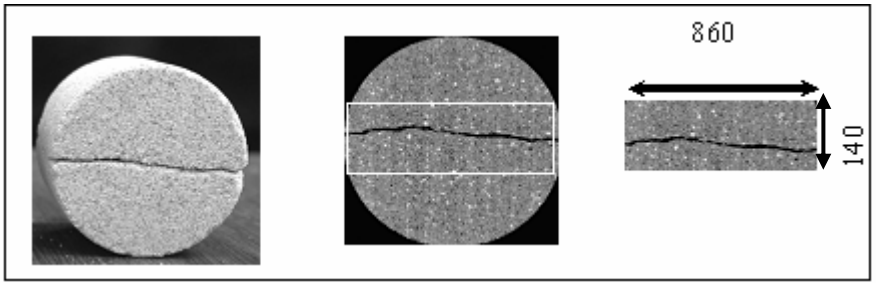

Figure 2: Left: a photograph of the fractured sample. Middle: a single CT slice showing the fracture the (dark linear feature) and the perpendicular bedding layers. Right: A cropped portion of the CT slice that was used to reduce the computational requirements.

Figure 3 shows a three-dimensional rendition of the fracture, in which the black areas represent the asperities (contact points) and gray the fracture volume itself. The three-dimensional reconstruction of the fracture aperture was subsequently used as the base for partitioning fluids and for determining fluid saturations during multiphase flow stages of the experiments. During the entire experiment, the core was held rigidly in place, with constant confining pressure, allowing registration of repeated volume scans for image subtraction operations. The solid matrix was removed from all image processing stages, thus providing a constraint for determining fluid/rock interfaces.

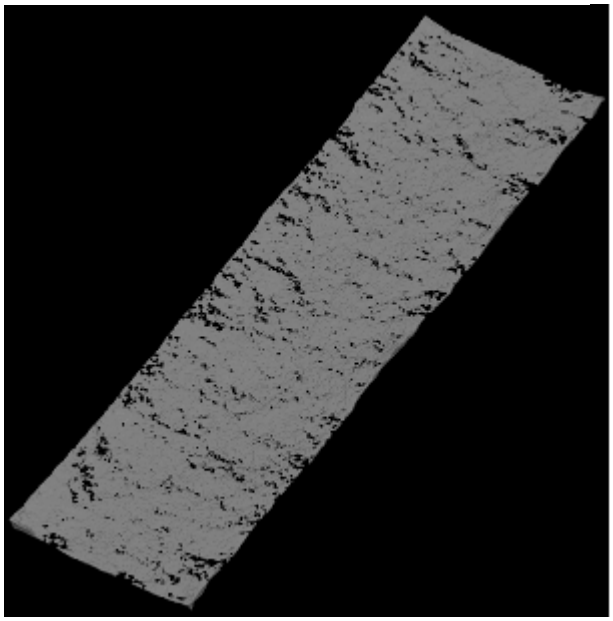

Figure 3: A three-dimensional rendition of the fracture in gray. The black spots are asperities.

For each confining stress the sample was dried and rescanned to create the base fracture volume.

Fracture Closure as a Function of Confining Stress

Figure 4 shows the fracture volume as a three-dimensional surface embedded in the rock matrix. The matrix and fracture are revealed in cross section in the figure's foreground. The figure compares fracture morphology at 3.5 MPa confining pressure (light gray, left) and at 17.2 MPa (white, right). The increased areas of darker gray matrix regions in the right hand figure denote the increase in the area of asperities as a result of the increase in net effective stress.

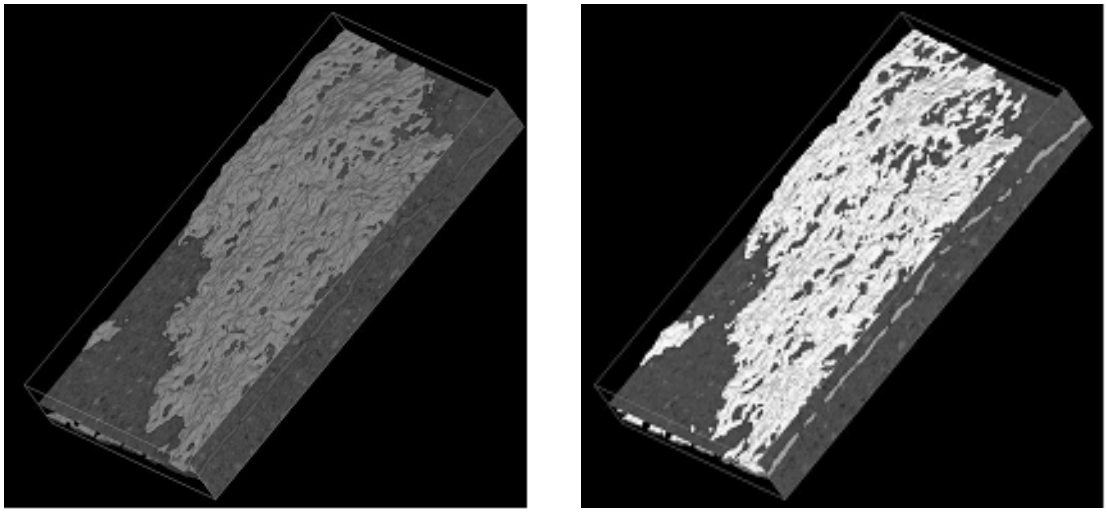

Figure 4: Left: A horizontal plane cutting through a three-dimensional rendition of the fracture volume at 3.5 MPa. Right: at 17.2 MPa.

These changes in fracture volume and asperity area can be quantified using the extracted digital fracture. At a confining pressure of 3.5 MPa, the computed fracture volume was 99.4 mm^3, with 1.58% of the fracture area occupied by asperities. At 17.2 MPa, the volume was 83.2 mm^3 with 5.69% asperity area. The average fracture aperture was 273 microns at 3.5 MPa confining pressure and 229 microns at 17.2 MPa confining pressure, a reduction of 15%. Figure 5 highlights the increase in the number of asperities, where black color corresponds to places with zero fracture aperture (less than 30 microns or 1 voxel).

Earlier studies, Gale (1987), Pyrak-Nolte *et al.* (1987), have suggested lognormal or gamma functions for fracture aperture distributions, highlighting the importance of the high-aperture tail of such distributions as representing channel flow. Zimmerman *et al.* (1991) suggested that the roughness of the fracture could be described by the ratio of the standard deviation of the mechanical aperture to the mean fracture aperture:

$$Roughness\ \ Factor = \frac{\sigma_m}{a_m} \qquad (1)$$

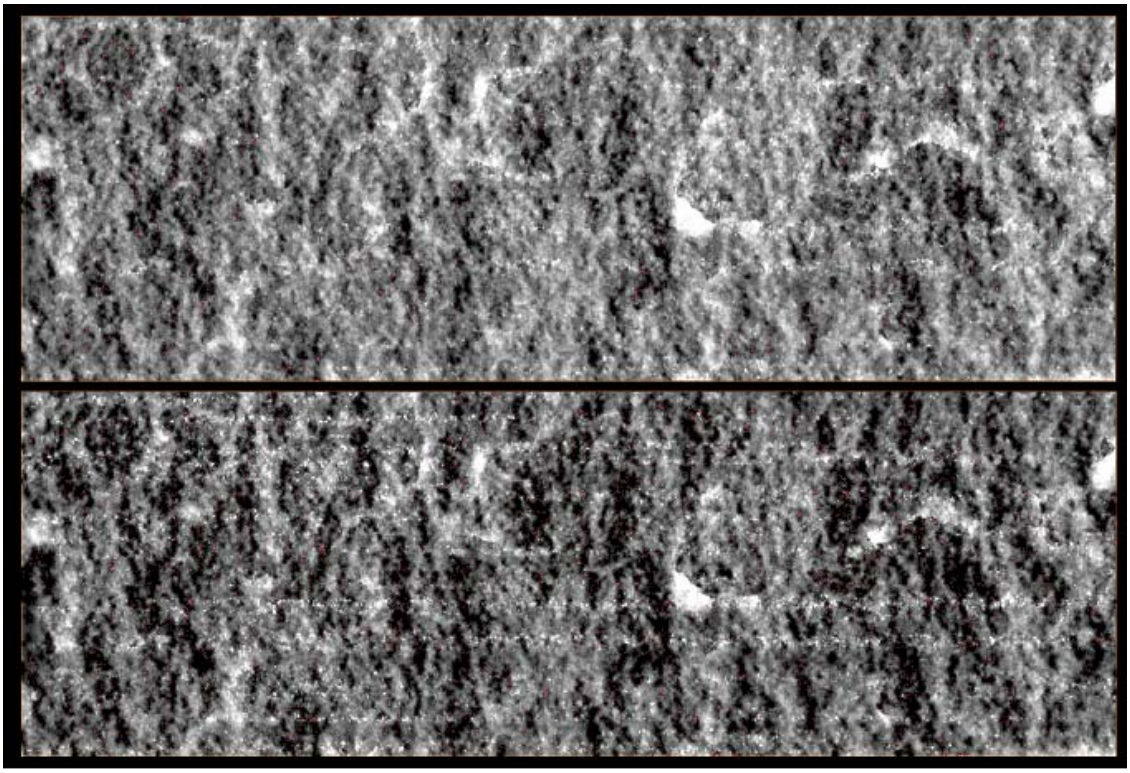

Figure 5: Two-dimensional renditions of the fracture showing asperities in black. Top: at 3.5 MPa closure stress. Bottom: at 17.2 MPa. The gray scale shows fracture apertures between 0 mm (black) and 1 mm in white. The image has been rotated 90 degrees (clockwise) so that flow is from left to right.

where σ_m represents the standard deviation of the aperture and a_m is the average aperture. A perfect parallel-plate model has uniform fracture aperture and therefore a zero standard deviation, leading to a zero roughness factor. For the 3.5- and 17.2-MPa confining pressure cases, the roughness factors were calculated as shown in Table 1. The data indicate an increase in the roughness parameter with confining stress, driven largely by decreased aperture.

Table 1: Roughness factor values

Confining Pressure (MPa)	a_m (microns)	σ_m (microns)	Roughness Factor
3.5	273	281	1.03
17.2	229	256	1.12

Mapping of Multi-phase Fluids in the Fracture

The x-ray CT data can also be used to map the distribution of separate fluid phases within the fracture. After the core was scanned dry and the digital fracture extracted, the core was vacuum saturated with water. Benzyl alcohol was injected at a rate of 6 cc/min until a state of irreducible water saturation was achieved.

The sample was rescanned in this condition. Using the previously extracted fracture volume, the fluids within the fracture were partitioned into oil and water fractions. Figure 6a shows a three-dimensional rendition of the oil in the fracture. Several drainage/imbibition loops were then performed, alternately injecting 100% oil and 100% water. At the end of oil flooding during one of these loops, the core was scanned at irreducible water saturation, and the oil fraction extracted as before (Figure 6b). The black color represents irreducible water and asperities. It is not effective to show in a gray scale the two fluid phases and one solid phase in three dimensions.

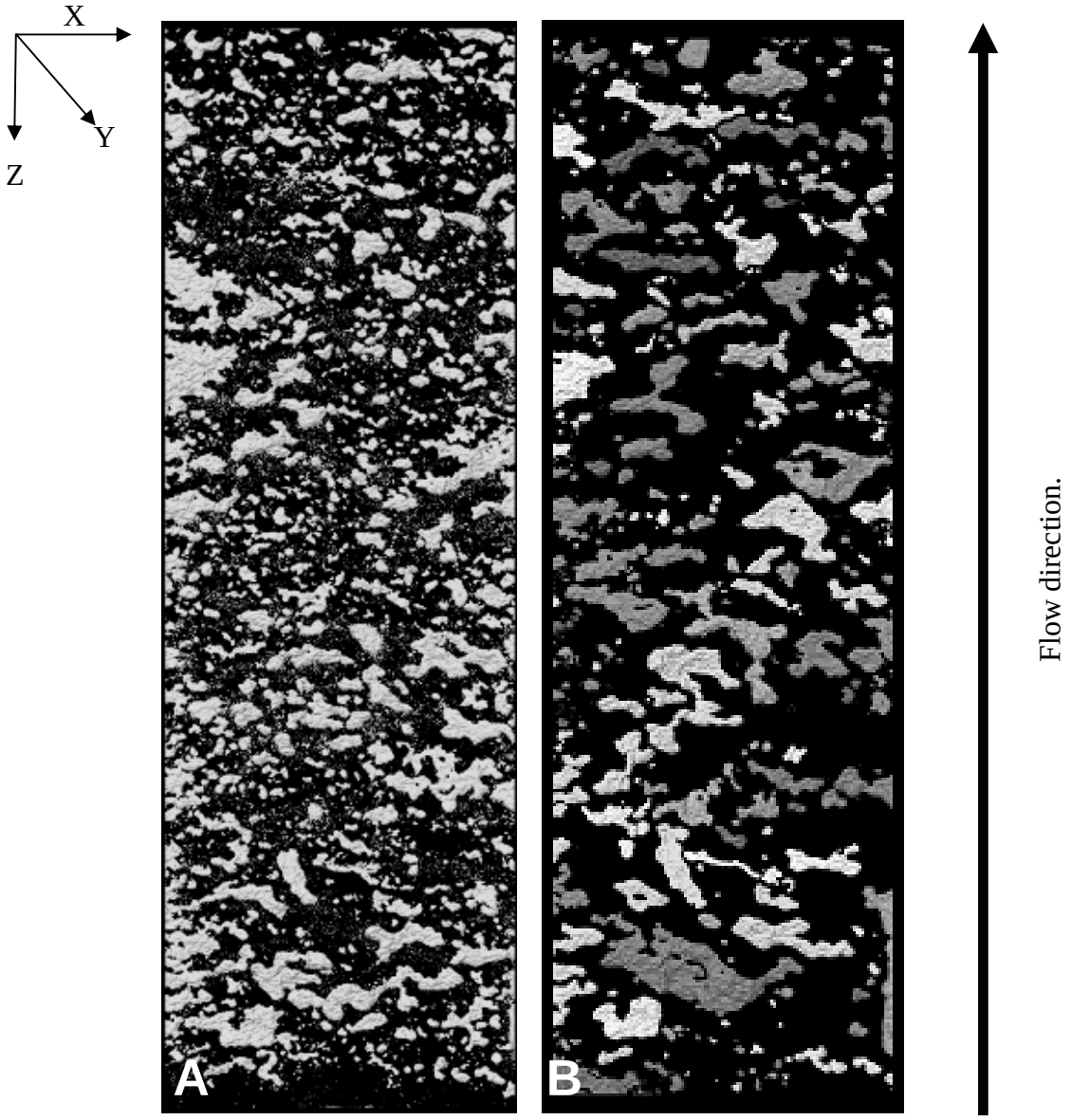

Figure 6: Three-dimensional rendition of the oil phase at residual water saturation. A: all oil volume, connected and unconnected, after the first oil injection phase. B: large non-connected oil globules after several water/oil fractional flow loops. Each image is 21.5 mm wide and 75.0 mm long.

In Figure 6a, a simple global threshold was applied to map all of the oil in the fracture. There is a wide range of oil globule sizes and many of the smaller ones appear to be disconnected. In Figure 6b, scanned under similar circumstances, a percolation algorithm was employed to select only oil-filled voxels connected to adjacent oil-filled voxels. We found large interconnected globules, disconnected from each other. To emphasize this, we have colored each isolated globule with a slightly different gray scale color. These two figures demonstrate the ability of the x-ray imaging technique presented in this paper to partition the fluid phases in the fracture.

Figure 7 is a summary comparison of oil and water distribution under both irreducible water (S_{wirr}) and residual oil (S_{or}) conditions. Figure 7A shows the fracture and the fluids at irreducible water saturation. Figure 7B shows the fluids at residual oil saturation. The irreducible water saturation is distributed in small volumes throughout the fracture (Figure 7A, S_{wirr}). The residual oil is in large, disconnected globules (Figure 7B, S_{or}).

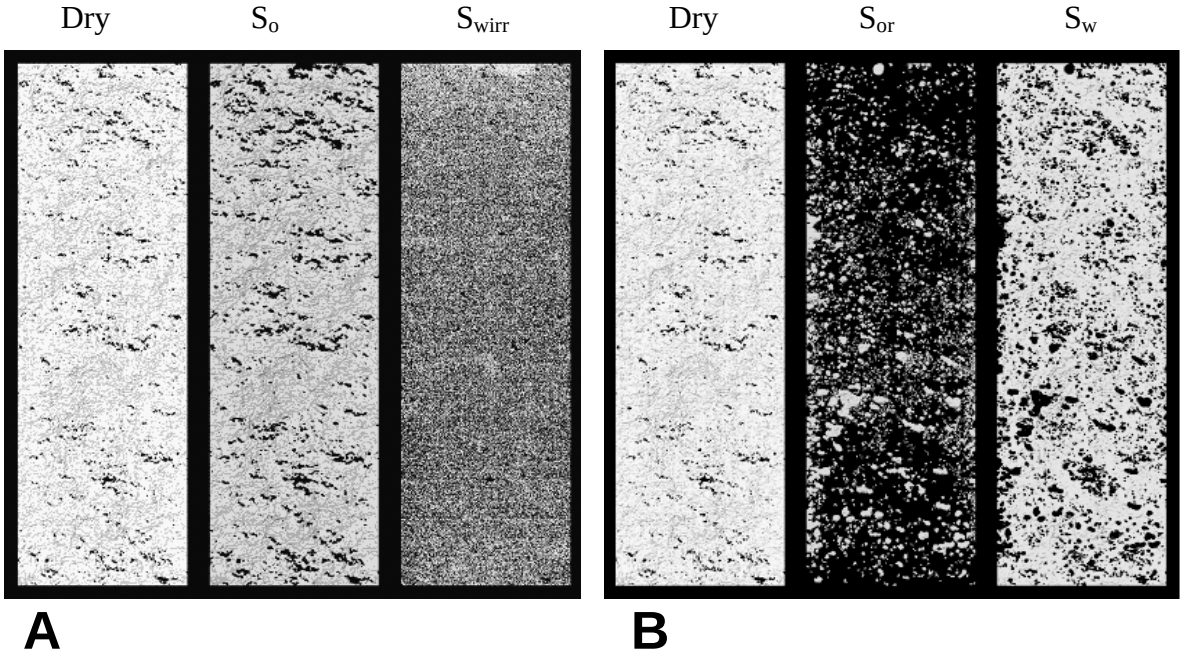

Figure 7: Fluids distribution maps after drainage and imbibition processes. Flow direction bottom-to-top. Each image is 21.5 mm wide and 75.0 mm long.
A: Three-dimensional renditions of: fracture volume (left), oil at irreducible water saturation (middle), water at irreducible water saturation. B: fracture volume (left), oil at residual oil saturation (middle), water at residual oil saturation.

The same techniques were used under three-phase conditions. At the end of the two-phase fluid flow experiments, a third phase (decane) was introduced. Three phases were simultaneously injected and fractional flow setting of 0.4/0.2/0.4 (water/benzyl alcohol/decane), and a total flow rate of 1 cc/min. The sample was allowed to equilibrate under gravitational forces for a period of eight hours, followed by a full CT scan. In this paper we focus on the equilibrated core condition where the overall fluid saturations were

25.7%, 41.6%, and 32.7% for water, benzyl alcohol, and decane, respectively. Figure 8 shows three-dimensional renditions of the fracture (Figure 8A), decane (8B), benzyl alcohol (8C), and water (8D). In this figure, only a third of the sample is shown in order to observe details of the saturation structure. The decane phase shown in figure 8B exhibits large globules associated with the regions of large fracture aperture. In some areas round isolated globules of decane can be seen (white arrow). The white circle on Figure 8B highlights a decane globule that is surrounded by the benzyl alcohol phase, shown in the white circle in Figure 8C. The decane globule appears as the black imprint denoted by the white arrow in Figure 8C. The fracture has a complicated topology, and the three-dimensional renditions of each phase are opaque. Thus if more than one phase is present when viewed from above (as these renditions are) then the same position will be gray in these diagrams. The multi-phase diagrams demonstrate the ability of high-resolution x-ray CT to quantify the structure of the fracture, as well as the partitioning of the phases that occupy it. This ability will allow us to better understand fracture-matrix mass transport, as well as in-fracture multi-phase flow.

SUMMARY AND CONCLUSIONS

High-resolution x-ray computed tomography has been applied to characterize fracture geometry as a function of closure stress and to map distribution of immiscible phases within the fracture under varying fluid injection conditions. An increase in closure stress from 3.5 to 17.2 MPa resulted in 15% decreases in both fracture volume and mean aperture and a corresponding increase in asperity contact area by a factor of 3.5. Quantitative image analysis of the fracture under multi-phase saturation conditions provides a rich field of investigation. For example, with water and “oil” phases present, flowing oil at irreducible water saturation, analysis of oil occupancy reveals that the oil is present largely in disconnected globules, despite the fact that it is the mobile phase. This shows that oil flow in a rugose fracture proceeds by a “snap-off” mechanism in which globules build up and migrate as a unit in an episodic fashion. The wetting phase on the other hand, despite its immobility, is well connected. The same techniques are illustrated in three-phase saturation conditions. This paper presents as a first step a quantitative and qualitative technique to map the occupancy of three phases in a fractured system. Further investigation using this technique is still on progress.

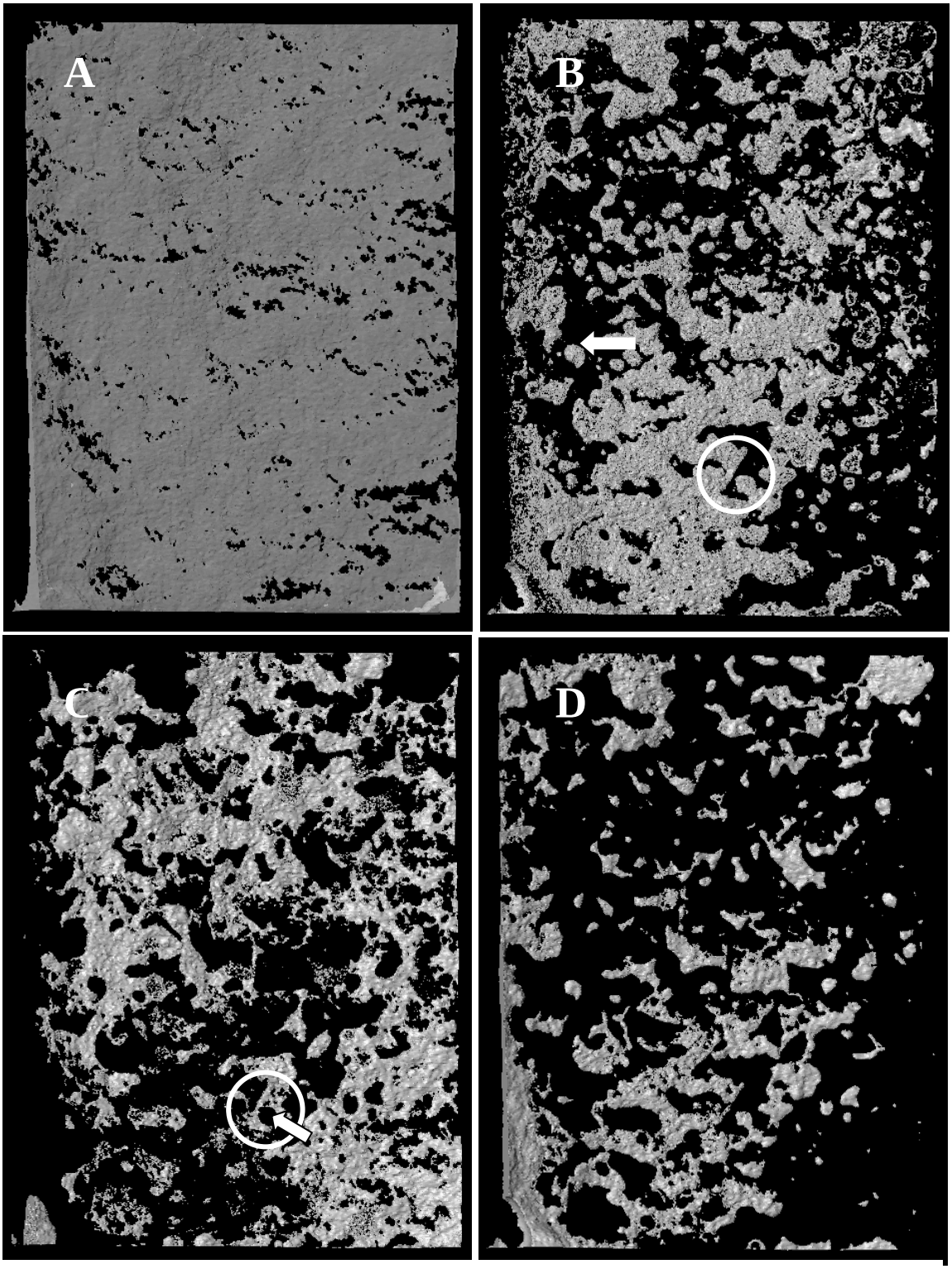

Figure 8: Three-dimensional renditions of the fracture occupied by three phases. A: the dry fracture volume. B: The decane phase (32.7%, the intermediate phase). C: The Benzyl alcohol phase (41.6%). D: The water phase (25.7%). Flow is from bottom to top. Only the first third of the sample is presented. Each image is 21.5 mm wide and 25.0 mm long.

REFERENCES

1. Alvarado, F. E., *Determination Of Mechanical And Hydraulic Behavior Of Tensile Fractures Under Multiphase Flow Using X-Ray Computed Tomography*, *PhD thesis*, The Pennsylvania State University, University Park, PA, (2005), 1-112.
2. Alvarado, F. E., A. S. Grader, O. Karacan, and P. M Halleck., "Visualization Of Three Phases In Porous Media Using Micro-Computed Tomography," *Petrophysics*, (2004), **45**, 6, 490-498.
3. Christiansen, R., C. Mayoral, and C. Pereira, "Capillary End Effects and Gas Production from Low-Permeability Formations," *Proceedings of the 19th International Symposium of the SCA*, Toronto, Canada, (2005).
4. Durham, W. B., W. L. Bourcier, and E. A. Burton, "Direct Observation of Reactive Flow In A Single Fracture," *Water Resources Research*, (2001) **37,** 1, 1-12.
5. Gale, J. E., "Comparison of Coupled Fracture Deformation and Fluid-Flow Models with Direct Measurement of Fracture Poro-structure and Stress-Flow Properties," *Proceedings of the 28th U.S. Symposium on Rock Mechanics*, Tucson, (1987), 1213-1222.
6. Gentier, S. and D. Hopkins, "Mapping Fracture Aperture As A Function Of Normal Stress Using A Combination Of Casting, Image Analysis And Modeling Techniques," *Int. J. Rock. Mech. and Min. Sci*., (1986) **34**, 3-4.
7. Lomize, G. M., *Flow In Fractured Rocks*, Gosenergoizdat, Moscow, (1951), 127 pp.
8. Louis, C., *A Study Of Groundwater Flow In Jointed Rock And Its Influence On The Stability Of Rock Masses*: *Imperial College Rock Mechanics Report No. 10*, Imperial College, London, (1969), 90 pp.
9. Pyrak-Nolte, L. J., L. R. Myer, N. G. W. Cook, and P. A. Witherspoon, "Hydraulic And Mechanical Properties Of Natural Fractures In Low Permeability Rock," *Proceedings of the 26th International Congress of Rock Mechanics*, Rotterdam, (1987), **1**, 225-232.
10. Tsang, Y. W. and C. F. Tsang, "Channel Model of Flow through Fractured Media," *Water Resources Research*, (1987) **23,** 3, 467-479.
11. Witherspoon, P. A., J. S. Y. Wang, , K. Iwai, and J. E. Gale, "Validity Of Cubic Law For Fluid Flow In A Deformable Rock Fracture, "*Water Resources Research*, (1980) **16**, 1016-1024.
12. Yeo, I. W., M. H. Freitas, and R. W. Zimmerman, "Effect of Shear Displacement On The Aperture And Permeability Of A Rock Fracture," *Int. J. Rock. Mech. Min. Sci.*, (1998) **35**, 1051-1070.
13. Zimmerman, R. W., S. Kumar, and G. S. Bodvarsson, "Lubrication Theory Analysis Of The Permeability Of Rough-Walled Fractures," *International Journal of Rock Mechanics and Min. Sci.*, (1991) **28**, 325-331.